

# Dual FGFR-targeting and pH-activable Smart Ruthenium-Peptide Conjugates for targeted therapy of Breast Cancer

João Franco Machado<sup>a,b</sup>, Marco Sá<sup>a,‡</sup>, Inês Pires<sup>c,‡</sup>, Miguel Silva<sup>b</sup>, Fernanda Marques<sup>b</sup>, Jaime A. S. Coelho<sup>a,d</sup>, Filipa Mendes<sup>b</sup>, M. Fátima M. Piedade<sup>d,e</sup>, Miguel Machuqueiro<sup>c,d</sup>, María Angeles Jiménez,<sup>f</sup> Maria Helena Garcia<sup>a,d</sup>, João D. G. Correia<sup>b\*</sup>, Tânia S. Morais<sup>a,d\*</sup>

<sup>a</sup> Centro de Química Estrutural, Institute of Molecular Sciences, Faculdade de Ciências, Universidade de Lisboa, Campo Grande, 1749-016 Lisboa, Portugal

<sup>b</sup> Centro de Ciências e Tecnologias Nucleares, Instituto Superior Técnico, Universidade de Lisboa, Estrada Nacional 10 (km 139,7), 2695-066 Bobadela LRS, Portugal

<sup>c</sup> BioISI – Biosystems & Integrative Sciences Institute, Faculdade de Ciências, Universidade de Lisboa, Campo Grande, 1749-016 Lisboa, Portugal

<sup>d</sup> Departamento de Química e Bioquímica, Faculdade de Ciências, Universidade de Lisboa, Campo Grande, 1749-016 Lisboa, Portugal

<sup>e</sup> Centro de Química Estrutural, Institute of Molecular Sciences, Instituto Superior Técnico, Universidade de Lisboa, Av. Rovisco Pais, 1049-001 Lisboa, Portugal

<sup>f</sup> Institute of Physical Chemistry Blas Cabreras (IQF-CSIC), Serrano 119, E-28006 Madrid, Spain.

‡ Both authors contributed equally to the work

Correspondence: TSM ([tsmorais@ciencias.ulisboa.pt](mailto:tsmorais@ciencias.ulisboa.pt)) and JGC ([jgalamba@ctn.tecnico.ulisboa.pt](mailto:jgalamba@ctn.tecnico.ulisboa.pt))

**Keywords:** Metastatic breast cancer · pH-sensitive drug delivery system · Anti-FGFR therapy · Ruthenium-cyclopentadienyl complex · Ruthenium-peptide conjugates

## Abstract

Dysregulation of Fibroblast Growth Factor Receptors (FGFRs) signaling has been associated with breast cancer, yet employing FGFR-targeted delivery systems to improve cytotoxic agents is still sparsely exploited. Herein, we report four new bi-functional ruthenium-peptide conjugates (RuPCs) with FGFR-targeting and pH-dependent releasing abilities, envisioning the selective delivery of cytotoxic Ru complexes to FGFR(+)-breast cancer cells, upon specific accumulation and controlled activation at the acidic tumoral microenvironment. The antiproliferative potential of the RuPCs and active Ru complexes was evaluated in four breast cancer cell lines with different FGFR expression levels (SK-BR-3, MDA-MB-134-VI, MCF-7, and MDA-MB-231) and in the normal human dermal fibroblasts (HDF) cell line, at pH 6.8 and 7.4 that mimics the tumor microenvironment and normal tissues/bloodstream, respectively. The RuPCs showed higher cytotoxicity in cells with higher level of FGFR expression at acidic pH. Additionally, RuPCs showed up to 6-fold higher activity in the FGFR(+) breast cancer lines compared to the normal line. The release profile of Ru complexes from RuPCs corroborates the antiproliferative effects observed. Remarkably, the cytotoxicity and releasing ability of RuPCs were shown to be strongly dependent on the peptide conjugation position in the Ru complex. Complementary molecular dynamic simulations and computational calculations were performed to help interpret these findings at

the molecular level. In summary, we identified a lead bi-functional RuPC that holds strong potential as a FGFR-targeted chemotherapeutic agent.

## Introduction

Breast cancer remains the most predominantly diagnosed cancer and the leading cause of female mortality worldwide, corresponding to 15.5% of annual cancer deaths in women.<sup>[1-3]</sup> Despite the great efforts on early diagnosis and treatment strategies, breast cancer recurrence and metastasis to the bones, lungs, liver, and brain renders it incurable, being the major reason for the current high mortality levels.<sup>[4-7]</sup>

Dysregulation of Fibroblast Growth Factor Receptors (FGFRs) signaling has been associated with the development and progression of various types of cancer, including breast cancer. Therefore, in recent years, it has emerged as a promising therapeutic target.<sup>[8-10]</sup> FGFRs are a family of receptor tyrosine kinases that play key roles in cell growth, survival, angiogenesis, differentiation, and repair of cellular tissues.<sup>[8-12]</sup> Aberrant activation or overexpression of FGFRs has been implicated in breast cancer pathogenesis, particularly in aggressive subtypes, being thus a marker of poor prognosis, as it is associated with the occurrence of metastases, early relapse, and resistance to standard therapy.<sup>[8,13,14]</sup> The overexpression of FGFRs by breast cancer cells comparatively to non-tumorigenic ones has paved the way for the exploration of FGFR inhibitors as potential new targeted therapies.<sup>[8-10,12]</sup> Although numerous ligands with high affinity and selectivity for FGFR, mainly peptides and small molecules, have already reached the clinical trials for several types of cancer,<sup>[9,12,15]</sup> none of them have shown to be sufficiently effective *in vivo* for breast cancer treatment.<sup>[8,13,15,16]</sup> FGFRs as components of the tumor microenvironment (TME) may also be used as molecular targets for drug delivery strategies, enhancing the precision and efficacy of anticancer drugs. Nonetheless, surprisingly, the use of specific FGFR ligands as delivery vectors for targeted anticancer therapy is yet scarcely explored. Indeed, only one antibody-drug conjugate was reported as a promising FGFR-targeted drug for advanced cancers, such as breast, colon, esophagus, liver, and pancreas, that reached phase I clinical trials.<sup>[17]</sup>

Several approaches for targeted delivery of metal complexes to tumors have been developed based on exploiting the unique molecular features of tumors.<sup>[18-26]</sup> In general, a tumor-targeting drug delivery system (DDS) comprises a tumor-recognizing delivery agent and a cytotoxic moiety, both connected directly or through a suitable linker to form a conjugate.<sup>[27-30]</sup> Peptides can bind to their targets with high specificity and efficiency, presenting low toxicity and immunogenicity which makes them good candidates for tumor-targeted DDS. Many peptide drug-conjugates have shown high potential in cancer chemotherapy,<sup>[23,31-38]</sup> in particular those systems containing metal complexes (such as Ru, Au, Fe, Co, Ir, Re ) as cytotoxic agents.<sup>[19,39-44]</sup> We have designed a tumor-targeting DDS based on the ruthenium-cyclopentadienyl complex [RuCp(PPh<sub>3</sub>)(2,2'-bipy)][CF<sub>3</sub>SO<sub>3</sub>] (**TM34**) combined to FGFR-targeting peptides. **TM34** itself showed to be highly potent *in vitro* against several cancers, in particular, the breast cancer cells (MFC7 and MDA-MB-231),<sup>[45-48]</sup> and the peptide was introduced as the vector to selectively deliver **TM34** to FGFR(+) breast cancer cells, sparing thus the non-tumorigenic tissues that have lower intrinsic levels of FGFR expression.<sup>[49]</sup> These three tumor-targeting ruthenium-peptide conjugates (RuPCs) were shown to be more cytotoxic against FGFR(+) breast cancer cells than against FGFR(-) cells. However, peptide conjugation also led to a considerable decrease in overall cytotoxicity compared to the parent complex **TM34**, impairing their further use. Herein, to improve the ability of these RuPCs to fight FGFR(+) breast cancers, we propose a novel strategy

that combines a **TM34** derivative complex with an FGFR-targeting peptide through a pH-responsive linker, that allows selective and controlled release of the Ru complex in its active form only at the target, triggered by the acidic pH of TME, boosting not only its selectivity but also its therapeutic activity. A schematic representation of the design rationale of this approach is illustrated in Figure 1. The four RuPCs differ in the conjugation position and/or the way the hydrazone, a well-known class of acid-labile structures for prodrugs, was synthesized. In this study, four pH-responsive ruthenium-peptide conjugates, named **RuPC1 – 4** (Figure 2), were developed, each composed of 3 building blocks, namely a Ru complex (cytotoxic agent), an FGFR-targeting peptide (targeting agent) and a hydrazone linker (pH-sensitive linker) formed by the reaction of the two previously mentioned moieties. The four RuPCs differ in the conjugation position and/or the way the hydrazone was synthesized. In fact, the hydrazone linker can be obtained by the reaction between a ketone-derivatized Ru complex (toxic agent) and a hydrazide-containing peptide (delivery agent) or vice-versa. Thus, here, we present the synthesis and characterization of four new organometallic Ru complexes functionalized with ketone and hydrazide groups on the Cp or bipyridine co-ligands (complexes **1**, **4**, **6** and **7**; Figure 2). These two positions had already been identified by our previous computational studies as the most suitable for derivatization and peptide conjugation without affecting the complex ability to interact with the cell membrane, a key process for the activity of **TM34**.<sup>[47,49]</sup> For the FGFR-targeted vector, we developed two new peptides based on the sequence VSPPLTLGQLLS, functionalized on the *N*-terminus with a 1,4-dioxo-pentanyl (peptide **P1**) or a (1-isobutyl)-4-hydrazide (peptide **P2**) groups, to allow the conjugation to the Ru complex. This sequence was known to bind with high affinity and specificity to the extracellular domain of FGFR and not be cytotoxic to the cancer cells, working in this approach only as a specific carrier.<sup>[49,50]</sup> The effect of metal conjugation on the 3-dimensional structure of the peptide was evaluated by NMR through the determination of the conformations of **P1** and **RuPC1** in aqueous solution. The dual effect of FGFR targeting and pH-activation of the new RuPC was evaluated *in vitro* against a panel of breast cancer cell lines with different FGFR expression levels at pH 6.8 and 7.4 that mimic the tumor microenvironment and normal tissues/bloodstream, respectively, and in a normal human dermal fibroblasts cell line at pH 7.4. The ability of the RuPCs to release the organometallic complexes in aqueous solutions at pH 6.8 or pH 7.4 was also evaluated by HPLC. Our findings suggest that the cytotoxicity and the release are strongly dependent on the position of the conjugation of the Ru complex to the peptide and the way that the hydrazone is constructed. Also, we identified a lead compound that holds the potential to be further studied for FGFR-targeted chemotherapy. The strategy presented herein holds promise for a new targeted therapeutic approach for the treatment of FGFR-related cancers.

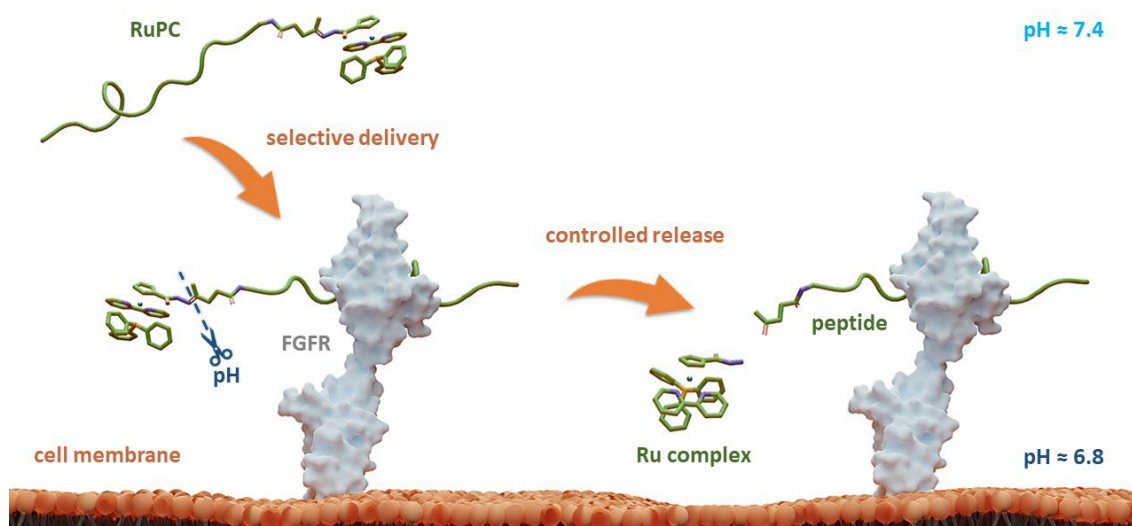


**Figure 2.** A conceptual overview of bi-functional ruthenium-peptide conjugates (RuPCs) based on targeting FGFR and a controlled release of the ruthenium active species at the acidic tumor microenvironment.

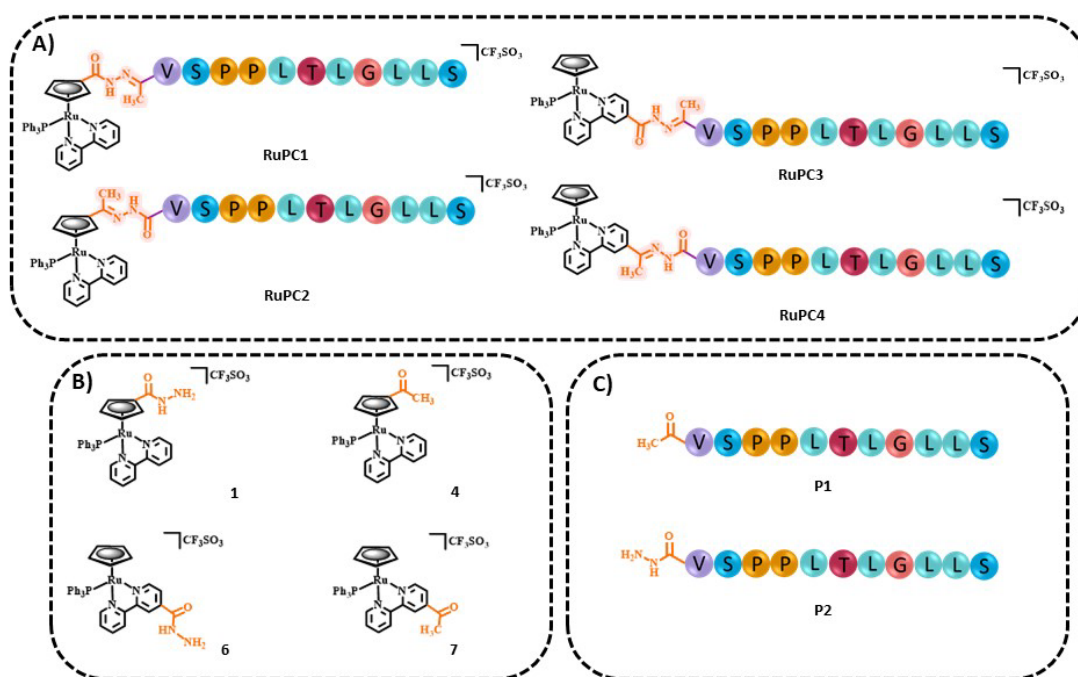


**Figure 1.** Chemical structures of (A) ruthenium-peptide conjugates (RuPC1 – 4), (B) active ruthenium complexes (1, 4, 6, and 7) and (C) peptides (P1 and P2)

## Results and Discussion

### Synthesis and characterization

Two new monofunctionalized bipyridine ligands were synthesized through a Stille coupling reaction. The precursor  $[\text{Ru}(\eta^5\text{-C}_5\text{H}_4\text{COCH}_3)(\text{PPh}_3)_2\text{Cl}]$  was obtained by reaction of sodium acetylcyclopentadienide with  $[\text{Ru}(\text{PPh}_3)_3\text{Cl}_2]$  in tetrahydrofuran. The final ketone/ester-derived complexes were obtained by heating, under reflux, the respective precursor complex with the corresponding bipyridine ligand in methanol. The hydrazide-derived complexes were prepared

by the reaction of the ester precursors with a large excess of hydrazine in ethanol under reflux. Detailed procedures, reaction schemes, and characterizations are provided in the Supporting Information. The structures of all complexes were confirmed by ESI-MS and  $^1\text{H}$ ,  $^{13}\text{C}$ ,  $^{31}\text{P}$  NMR, FT-IR, and UV-vis spectroscopies. The purity of all complexes was assessed by percentual elemental analysis, and HPLC (only for compounds **1**, **4**, and **6**). Single crystals of complexes **1**, **3** (used as precursor of **4**), and **4** suitable for SCXRD were obtained by the diffusion of diethyl ether in a dichloromethane solution of each complex. Figure 3 shows the molecular structures of the compounds and the selected bond lengths and angles are provided in Supporting Information.

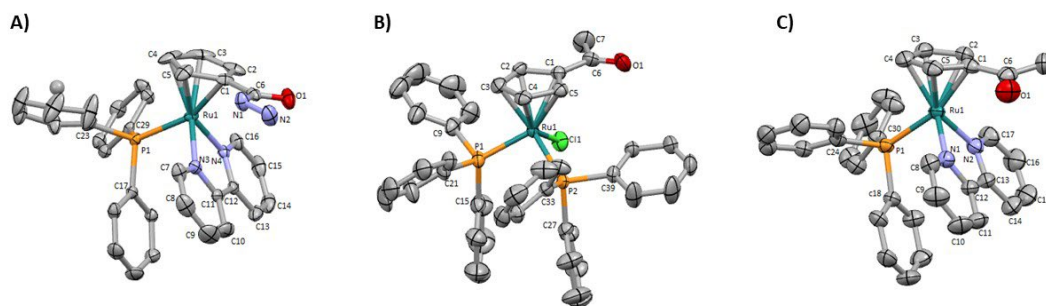


**Figure 3.** Molecular diagrams for (A)  $[\text{Ru}(\eta^5\text{-C}_5\text{H}_4\text{CONHNH}_2)(\text{PPh}_3)(2,2'\text{-bipy})]^+$  (**1**), (B)  $[\text{Ru}(\eta^5\text{-C}_5\text{H}_4\text{COCH}_3)(\text{PPh}_3)_2\text{Cl}]$  (**3**) and (C)  $[\text{Ru}(\eta^5\text{-C}_5\text{H}_4\text{COCH}_3)(\text{PPh}_3)(2,2'\text{-bipy})]^+$  (**4**).

These monocyclopentadienyl ruthenium complexes present the usual “three-legged piano stool” geometry around the metal as confirmed by X–M–P angles close to  $90^\circ$  (X = N or Cl), with the remaining Cp–M–X (X = N or P) angles between  $121.370(19)^\circ$  and  $130.16(13)^\circ$ . Complexes **1** and **4** crystallize in the monoclinic crystal system in the P 21/c and P 21/n space groups respectively and complex **3** crystallizes the triclinic crystal system in the P1 $^-$  space group. For complexes **1** and **4** the asymmetric unit consists of a cationic complex and  $\text{CF}_3\text{SO}_3^-$  anion, while for compound **3** the asymmetric unit consists of the neutral complex and a water molecule.

Furthermore, the stability of complexes **1**, **4**, **6**, and **7** was evaluated in aqueous and organic solutions by UV-vis spectroscopy over 24 h to assess their suitability for further conjugation to peptides and biological studies. The assays were performed in 100 % dimethyl sulfoxide (organic solution) and 5 % dimethyl sulfoxide / 95 % cell culture medium DMEM+GlutaMAX-I (aqueous solution) at room temperature. All complexes showed to be stable under these conditions, as the acquired electronic spectra did not display any significant variation over time regarding the number, type, shape, nor maximum absorbance of the bands ( $\Delta A_{\text{max}} < 8\%$  for  $\pi \rightarrow \pi^*$  and MLCT bands).

The evaluation of the lipophilicity of a complex intended to be used for biomedical applications is among the primary steps of the drug development process. This important physicochemical property has a considerable impact on the pharmacokinetics and pharmacodynamics profiles of the complex, as well as a strong influence on its drug formulation. Particularly, lipophilicity influences the ability of the complex to interact with drug targets and cross-cell membranes, as well as its solubility, tissue permeability, cytotoxicity/bioactivity, and general toxicity.<sup>[51]</sup> The partition coefficients in n-octanol/water of complexes **1**, **4**, **6**, and **7** as well as the reference complex  $[\text{Ru}(\eta^5\text{-C}_5\text{H}_5)(\text{PPh}_3)(2,2'\text{-bipy})][\text{CF}_3\text{SO}_3]$  (**TM34**), were estimated by the shake-flask method.<sup>[52]</sup> Compared to **TM34**, which showed moderate lipophilicity ( $\log P = 1.1 \pm 0.05$ ), all the

derivatizations led to a slight decrease of the lipophilicity (**1**: Log P = 0.43 ± 0.01; **4**: log P = 0.25 ± 0.02 and **7**: log P = 0.83 ± 0.03), with the exception for compound **6** (log P = 1.55 ± 0.06), with the bipyridine ligand functionalized with a hydrazide group, that is slightly more lipophilic than **TM34**.

The bioavailability of small (metallo)drugs to tumor sites is often limited due to their low efficiency in achieving selectivity at the tumor site, thus attaching specific peptides could enhance drug accumulation at the target.<sup>[18,53,54]</sup> The syntheses of the novel pH-responsive Ru-peptide conjugates (**RuPC1** – **RuPC4**) comprised three main steps: (i) preparation of the organometallic complexes **1**, **2**, **6**, and **7**; (ii) synthesis and purification of two new peptides derived from the FGFR-targeting peptide VSPPLTLGQLLS,<sup>[55–57]</sup> where the *N*-terminus was functionalized with a 1,4-dioxo-pentanyl (peptide **P1**) or a (1-oxobutyl)-4-hydrazide (peptide **P2**) group; and (iii) conjugation of each organometallic complex with the respective peptide through the formation of a hydrazone bond. The peptides were prepared on a Rink amide resin by ultrasound-assisted solid-phase peptide synthesis (US-SPPS), according to our previously reported methodology.<sup>[50]</sup> Peptide **P1** was *N*-functionalized with a ketone group by treating the resin with levulinic acid. Analogously, *N*-derivatization of **P2** with the hydrazide group was performed in two steps, first by treating the resin with succinic anhydride, and then by reaction of the product with fmoc-hydrazine, followed by final fmoc deprotection. It is important to mention that treating the resin with an excess of succinic anhydride or for long periods, during the first step, led to the polymerization of **P2** through the formation of the respective poly succinate ester. After final deprotection, peptide cleavage, and purification procedures both peptides were obtained with *C*-terminal amide with > 98 % purity. The four new RuPCs were synthesized by reacting the hydrazide-derived complex with the respective ketone-derived peptide, or vice-versa (Figure 2A). The RuPCs were obtained in high purity (> 97 %). Interestingly, **RuPC1**, **RuPC3**, and **RuPC4** were obtained as a 1:1 mixture of *E/Z*-hydrazone isomers, whereas for **RuPC2** only one was found. The six new compounds **P1**, **P2**, **RuPC1** - **RuPC4** were characterized by analytical HPLC and ESI-MS, which results corroborate the proposed structures. The whole synthesis procedures (peptides and RuPCs), reaction schemes, and characterizations are provided in the Supporting Information.

The 3-dimensional conformation of a peptide can provide insights into its physicochemical and biological properties.<sup>[58–60]</sup> We determine the conformation of peptide **P1** and the structural impact of the conjugation to the metal (**RuPC1**) by NMR. The 2D <sup>1</sup>H-<sup>1</sup>H-TOCSY spectrum of **P1** exhibited a set of intense cross-peaks (Figure S3A), which corresponds to the major species, as well as some weak cross-peaks. This is common for Pro-containing peptides due to the *cis-trans* isomerization of the X-Pro bonds.<sup>[61,62]</sup> Since the sequence of peptide **P1** contains two Pro residues, up to four species could be present in solution, i.e., *trans-trans*, *cis-trans*, *trans-cis*, and *cis-cis*. We observed that the two Pro residues are *trans* in the major species since the differences between the chemical shifts of the <sup>13</sup>C<sub>β</sub> and <sup>13</sup>C<sub>γ</sub> carbons ( $\Delta^{\beta\gamma} = \delta^{C\beta} - \delta^{C\gamma}$ , ppm) are small ( $\Delta^{\beta\gamma} < 5$  ppm).<sup>[61,62]</sup> Sequential NOEs between the H<sub>α</sub> proton of Ser2 and the H<sub>δδ'</sub> protons of Pro3 and between the H<sub>α</sub> proton of Pro3 and the H<sub>δδ'</sub> protons of Pro4 confirm that the rotamer state of both X-Pro bonds is *trans*. Concerning the minor species, only some signals belonging to V1 and S2 of one of them could be assigned. Based on the intensities of equivalent cross-peaks, the percentages of major (*trans-trans*) and minor species are 90 and 10 %, respectively. The NMR spectra of conjugate **RuPC1** showed several sets of cross-peaks for residues Val1, Ser2, Pro3, and Pro4, two of the sets of similar intensities (their relative percentages are 47±4 and 53±4 according to the intensities of 19 equivalent cross-peaks). In the 2D <sup>1</sup>H-<sup>1</sup>H-TOCSY spectrum

(Figure S3B), four  $^1\text{H}_\alpha$ - $^1\text{H}_\text{N}$  cross-peaks are observed for Val1. According to the intensities of these Val1 cross-peaks, the percentages are 47, 40, 9 and 4 %. Very likely the two major species correspond to isomers at the conjugate moieties, whereas the minor species will correspond to each of those isomers and a *cis* Pro rotamer. As in the free peptide, based on the small value of the difference between the chemical shifts of the  $^{13}\text{C}_\text{b}$  and  $^{13}\text{C}_\text{g}$  carbons of the two Pro residues indicates that the two X-Pro bonds in the two major species are *trans*. We also analyze whether the major species of peptide **P1** and conjugate **RuPC1** form some preferred conformation, we examined the plots of  $^1\text{H}_\alpha$  and  $^{13}\text{C}_\alpha$  chemical shift deviations ( $\Delta\delta = \delta^{\text{observed}} - \delta^{\text{random coil}}$ , ppm) as a function of peptide sequence (**Figure 4**). It is noticeable that the profiles displayed by **P1** and **RuPC1** are almost identical, which indicates that conjugation does not affect the conformational behavior of the peptide moiety. Excluding the Pro-preceding residues, which exhibit their characteristic large values,<sup>[63]</sup> most chemical shift deviations are within the random coil range, which points out to mainly disordered peptides. However, the stretch of consecutive negative  $\Delta\delta_{\text{H}\alpha}$  and positive  $\Delta\delta_{\text{C}\alpha}$  displayed by residues 7-10 suggests low populated helical conformations (estimated helix percentage is about 16%). The complete assignments are provided in the Supporting Information.

### **Cytotoxic activity in FGFR-Positive/negative breast cancer cells**

Since the RuPCs were designed as a bi-functional system with FGFR targeting and pH-activation, we envisioned that treatment of FGFR(+)-cancer cells at an acidic pH with RuPCs could lead to a higher inhibition of proliferation. Therefore, we evaluated the cytotoxic properties of the new conjugates, peptides, and complexes in a panel of breast cancer cell lines with different FGFR expression levels, namely SK-BR-3, MDA-MB-134-VI, MCF-7, and MDA-MB-231, at pH 6.8 and 7.4 that mimics the tumor microenvironment and normal tissues/blood-stream, respectively.<sup>[64]</sup> SK-BR-3 and MDA-MB-231 cell lines are metastatic breast cancer models, while MCF-7 and MDA-MB-134-VI are hormone-dependent breast cancer models.<sup>[65-67]</sup> Our immunoblotting studies showed that SK-BR-3 and MDA-MB-134-VI had the highest level of FGFR expression, followed by MCF-7, while for MDA-MB-231 no expression was detected (data not shown). For this purpose, the conjugates, free complexes, and peptides were incubated in phosphate buffer solutions at pH 6.8 and 7.4 for 48 h, before exposing the different cell lines to increasing concentrations of these solutions (0.1 – 50  $\mu\text{M}$ ), to determine their viability after an additional 48 h of incubation. The first screening in SK-BR-3 and MDA-MB-134-VI cells showed that both peptides **P1** and **P2** are not active at the concentrations tested (up to > 100  $\mu\text{M}$ ; Table 1). In general, all the conjugates and free organometallic complexes were shown to be highly cytotoxic in all the tested lines, with  $\text{IC}_{50}$  values in the micromolar range (Table 1 and Figure S4). The cytotoxicity is strongly dependent on the position of the conjugation of the peptide to the Ru complex. In fact, when the peptide conjugation is on the Cp ring the RuPCs were shown to be more cytotoxic than the free Ru complexes, while the opposite effect was observed for RuPCs conjugated via bipyridine ligand. As expected, except for **RuPC3**, the  $\text{IC}_{50}$  of the conjugates showed to be dependent on the FGFR expression level and the pH value, while the activity of free complexes does not correlate with any of these factors. Conjugates **RuPC1**, **RuPC2**, and **RuPC4** were shown to be up to 6 times more active in cell lines that express the FGFR receptor than in the one that does not overexpress it. This effect is particularly evident at pH 6.8 with the higher difference observed for **RuPC1**. On the contrary, for the respective free complexes there was no evident correlation between the level of FGFR expression and their cytotoxic activity, as expected. Thus, these data

suggest a relevant role of the peptide in the targeted delivery of the complexes to breast cancer cells overexpressing this receptor.

Regarding the pH, **RuPC1** was up to 4-fold more cytotoxic at pH 6.8, which mimics the tumor microenvironment, than at pH 7.4 in all cancer cell lines, while **RuPC2** does not appear to be very significant among the two pH values tested. When the peptide is conjugated to bipyridine, a completely different behavior is observed. Unexpectedly, **RuPC3** is more cytotoxic at pH 7.4 than 6.8, with this effect being more evident in MDA-MB-134-VI and MDA-MB-231 cells. For **RuPC4**, at pH 7.4, this conjugate showed a cytotoxic activity similar to that of free Ru complex **7**. Also, unexpectedly, at pH 6.8, a significant loss of activity of this conjugate was observed in all cell lines studied, which was up to 7 times lower than its activity at pH 7.4. The respective free complexes did not show significant differences between the two pH values tested. Regarding the free Ru organometallic complexes, it is observed that compounds functionalized with a ketone group are more cytotoxic than those containing a hydrazide group. As observed for RuPCs, also the cytotoxicity of free complexes is dependent on the position of the functionalization.

**Table 1.** IC<sub>50</sub> values (μM) of the conjugates (RuPC1 – 4) and the free Ru complexes (1, 4, 6 and 7) for breast cancer cells with different FGFR expression levels: MDAMB134\_VI (++) , SKBR3 (++) , MCF7 (+) and MDAMB231 (-).

Compounds	IC <sub>50</sub> (μM) 48h							
	MDAMB134_VI		SKBR3		MCF7		MDAMB231	
	pH6.8	pH7.4	pH6.8	pH7.4	pH6.8	pH7.4	pH6.8	pH7.4
<b>1</b>	25±5.3	23±5.0	45±12	40±11	12±2.0	12±2.0	38±8.2	34±7.6
<b>RuPC1</b>	7.4±1.4	17.4±5.0	7.9±1.7	14±3.5	2.1±0.7	8.5±2.3	12.9±3.1	26.4±9.8
<b>4</b>	10.2±3.8	12.8±4.1	7.5±1.9	7.5±1.9	2.5±0.6	3.0±0.6	10.2±1.3	11.3±1.5
<b>RuPC2</b>	6.2 ±1.9	5.9±1.9	3.3±0.7	4.3±0.8	1.1±0.3	1.7±0.4	4.0±0.7	7.7±2.5
<b>6</b>	19.8±2.8	21.2±2.9	7.1±1.2	6.5±1.2	4.3±0.9	3.1±0.5	20±3.2	20.3±2.3
<b>RuPC3</b>	37.4±6.8	26.7±6.2	11.4±2.1	10.6±2.2	10.4±3.3	9.5±3.1	36.9±5.8	23.4±3.4
<b>7</b>	6.4±1.4	6.2±1.4	3.9±1.3	2.7±0.6	1.9±0.4	2.0±0.4	4.9±1.0	3.9±0.8
<b>RuPC4</b>	17.1±2.3	4.1±1.1	21.8±5.5	3.9±0.8	9.7±1.9	2.4±0.6	47.7±6.5	6.7±1.2
<b>Peptides</b>	>100		>100		>100		>100	

Since fibroblasts are cells present in all tissues of the human body that naturally express FGFRs,<sup>[68–72]</sup> to anticipate possible adverse effects due to cytotoxicity in healthy tissues, we evaluate the *in vitro* toxicity of the two most promising conjugates **RuPC1** and **RuPC2** and their respective free Ru complexes (**1** and **4**) in the normal human dermal fibroblasts (HDF) cell line (Table 2). The free Ru complexes are more active in the normal cell line when compared with all the breast cancer cell lines (SI < 0.8), except for MCF-7. In MCF-7, complex **4** showed a selectivity index of 2, while for complex **1** the IC<sub>50</sub> is in the same concentration range as in the normal cell lines, which evidences the low intrinsic selectivity of free complexes. However, after conjugation of the peptide, both conjugates showed an opposite behavior as expected, being less active in normal cells than in cancer cells (1.2 < SI < 7.3). The sole exception is **RuPC2** in MDA-MB-134-VI cells, where its cytotoxicity is in the same concentration range as in the normal cell (SI = 1.0). In fact, for the other three cell lines, **RuPC1** was shown to increase the selectivity of complex **1** between 4 and 10 times, whereas **RuPC2** was only 3 to 4 times more selective than the respective complex **4**. It is also noteworthy that both conjugates show up to 6-fold higher SI values in the FGFR(+) breast cancer lines compared to the FGFR(-) normal line.



**Table 2.** IC<sub>50</sub> values (μM) in the normal cell line HDF at pH 7.4 and selectivity index values calculated for conjugates **RuPC1** and **RuPC2**, as well as respective free complexes **1** and **4**, referred to the IC<sub>50</sub> of these compounds in the normal cell line HDF at pH 7.4 compared to their cytotoxicity in the breast cancer cell lines SK-BR-3, MDA-MB-134-VI, MCF-7, and MDA-MB-231 at pH 6.8.

Compounds	IC <sub>50</sub> (μM) HDF	SI (healthy pH7.4 / tumoral pH6.8)			
		HDF/SK-BR-3	HDF/MDA-MB-134-VI	HDF/MDA-MB-231	HDF/MCF-7
<b>1</b>	10.1±2	0.2	0.4	0.3	0.8
<b>RuPC1</b>	15.3±3.5	1.9	2.1	1.2	7.3
<b>4</b>	4.4±1.3	0.6	0.4	0.4	1.8
<b>RuPC2</b>	5.7±1.4	1.7	0.9	1.4	5.2

### Drug release behavior

To evaluate the ability of the RuPCs to release the organometallic complexes in an aqueous solution, **RuPC1** - **RuPC3** were treated with phosphate buffer solutions at pH 6.8 or pH 7.4 that mimics the tumoral microenvironment or the bloodstream/healthy tissues respectively. A small percentage of acetonitrile (10 %) was used as a co-solvent to fully solubilize the conjugates at the working concentration (0.5 mg/mL). The release profiles were monitored by HPLC over 50 hours. Interestingly, each of them showed a different behavior. For **RuPC1**, at pH 6.8, the chromatographic peak for the Ru-peptide conjugate continuously decreased as the incubation time increased (Figure 5A). Simultaneously, a proportional increase of the signals of **P1** and complex **1** was observed over the same period. After 24h, a new peak with a retention time of 14.1 min appeared, the new product was characterized as the complex resulting from the hydrolysis of complex **1** to a carboxylic acid [Ru(η<sup>5</sup>-C<sub>5</sub>H<sub>4</sub>COOH)(PPh<sub>3</sub>)(2,2'-bipy)][CF<sub>3</sub>SO<sub>3</sub>] (**TM281**), previously developed and reported by us.<sup>[49]</sup> Indeed, complex **1** was released from **RuPC1** in an exponential-like way during the first 6 h, for a quantitative evaluation (Figure 5B), after 6 h the release of complex **1** from **RuPC1** was calculated in 41 %. With a prolonged incubation period, free complex **1** was continuously released, reached 79% after 24 h, and an almost complete release at 50 h (97 %). These results suggest the successful hydrolysis of the conjugate into the respective free peptide and complex in its active form, with a small amount of it being later hydrolyzed to **TM281**. The hydrolysis of complex **1** to **TM281**, may in part explain the lower cytotoxicity of complex **1**, compared to complex **4**, since **TM281** has already been shown to have a low cytotoxic potential.<sup>[49]</sup> To be used as a potential targeted therapy the drug delivery system should be stable under non-tumoral conditions. Thus, at pH 7.4, mimicking the bloodstream and healthy tissues, a similar behavior for **RuPC1** was observed (Figure 5A), but at a significantly lower rate of release. As shown in Figure 5B, at the pH of non-tumorigenic tissues, only a quarter part of complex **1** was released under a 50 h period following linear kinetics (release rate at 24 h = 14 % and 50 h = 26 %), suggesting that **RuPC1** shows a pH-dependent controlled drug release profile compatible with the desired application. Surprisingly, **RuPC2**, which contains a mirrored hydrazone bond relative to that of **RuPC1**, showed limited drug release ability under analogous conditions. At both pH values, the chromatographic peak relative to this conjugate decreased very slowly, with a proportional slow release of **P2** and complex **4** (Figure 5C). Indeed, from Figure 5D, we can observe that after the first 6 h only 6 % of complex **4** was released from **RuPC2**, achieving a plateau after 24 h with a release of 15 %, which did not significantly increase with longer incubation time. Analogously, at pH 7.4, only a very small

amount (9 %) of complex **4** was released within 50 h of incubation. On the contrary, for **RuPC3**, with the peptide conjugated through the bipyridine ligand, a high release rate of complex **6** was observed (Figure 5E), to the same extent for both pH values. For quantitative evaluation (Figure 3F), a release of 60 % was observed after 6 h, and after a prolonged incubation period, free complex **4** was continuously released reaching 99.5 % after 50 h. Meanwhile, a new peak with a retention time of 11.8 min emerged and significantly intensified, which was identified by ESI-MS as the product from the hydrolysis of complex **4** to the carboxylic acid derivatized complex -  $[\text{Ru}(\eta^5\text{-C}_5\text{H}_5)(\text{PPh}_3)(2,2'\text{-bipy-COOH})][\text{CF}_3\text{SO}_3]$  (product not isolated). Unfortunately, it was not possible to evaluate the release profile of the active complex **7** from **RuPC4** since we could not find an analytical HPLC method capable of eluting and separating both the conjugate **RuPC4** and the free peptide and complex **7**. The pH-responsiveness of the conjugates can explain the differences observed in the cytotoxic profile of each RuPC, and highlight the need for the complex to be released from the conjugate, i.e., to be present in its active form and increase its efficacy, as it was also reported for other drug delivery systems.<sup>[19,49]</sup> Indeed, whereas **RuPC2** was only slightly more active than complex **4** in the breast cancer cell lines, **RuPC1** showed to be significantly more active (up to 5-fold) than the respective free complex **1** at pH 6.8. Thus, the

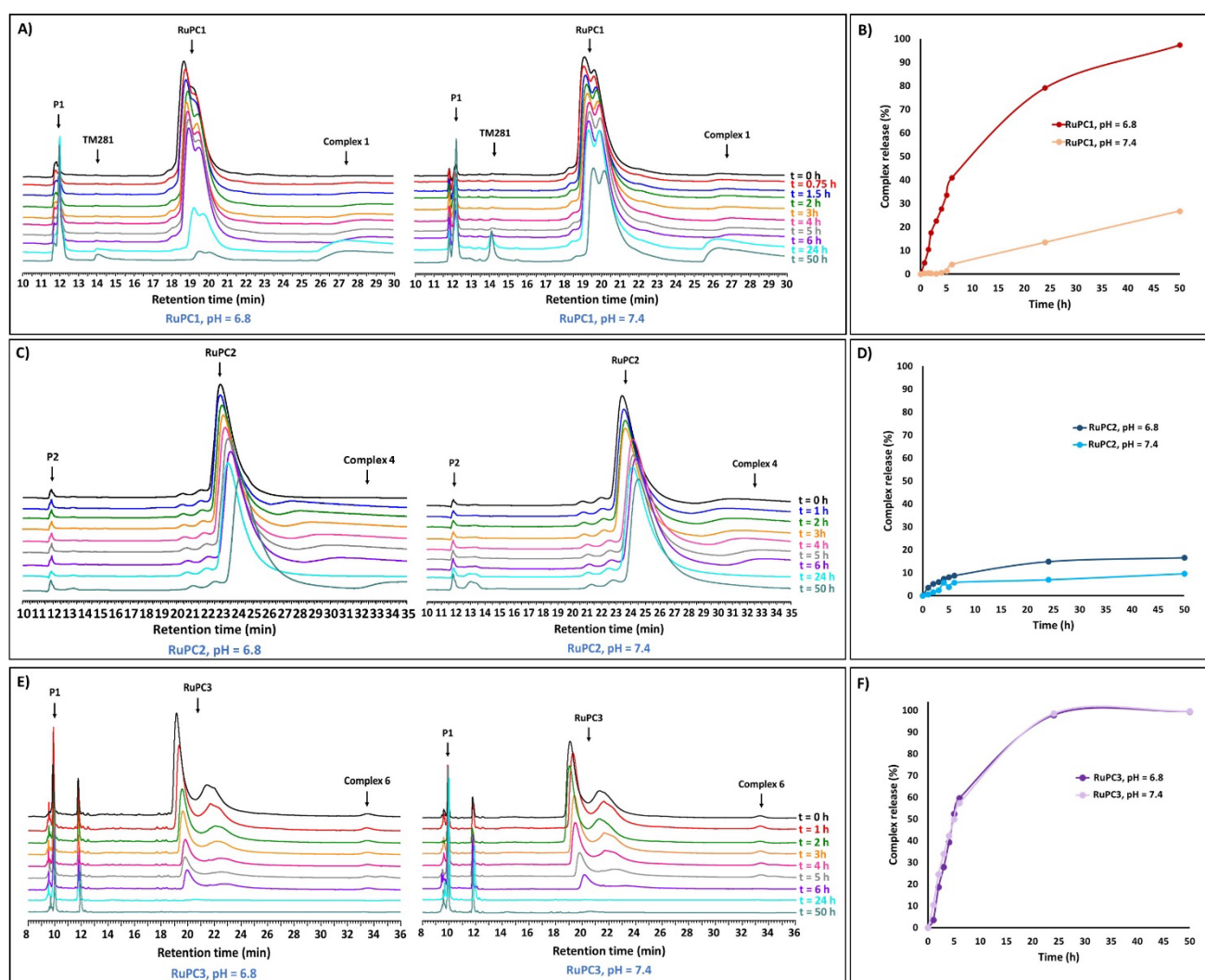


**Figure 4.** pH dependent Ru complex release profiles under pH 6.8 (tumor microenvironment) and pH 7.4 (bloodstream/healthy tissues). Time course of complexes **1**, **4** and **6** release profile from **RuPC1**, **RuPC2** and **RuPC3**, respectively, monitored by RP-HPLC at intervals: 0, 1, 2, 3, 4, 5, 6, 24, and 48 h (A, C, E); Percentage of complexes **1**, **4** and **6** from **RuPC1**, **RuPC2** and **RuPC3**, respectively (B, D, F).

overall results indicate that **RuPC1** has a drug profile adequate for the controlled release of the active organometallic complex at the tumor site, whereas **RuPC2** and **RuPC3** do not.

To understand the relative stability observed with **RuPC1** and **RuPC2**, we studied the hydrolysis of these hydrazones with density functional theory at M06-2X/def2-TZVPP,SDD(Ru)//M06-2X/6-31G(d,p),SDD(Ru) level of theory. We assumed that the rate of hydrolysis is mainly dependent on the proton affinity (PA)<sup>[73,74]</sup> and electrophilicity of the corresponding iminium ions. The calculated PA ( $\Delta$ PA is 1.0 kcal mol<sup>-1</sup>) and Fukui indices  $f^+$  are greater in **RuPC1** compared to **RuPC2**, suggesting that **RuPC1** is more basic and the corresponding iminium ion more electrophilic than that of **RuPC2**. These results agree well with the experimental observations and, together with similar conclusions obtained for truncated model substrates (see Figures S6 – S9), suggest that alkyl hydrazones are more easily hydrolyzed than aryl hydrazones.

### **Membrane Interactions and Permeability from MD Simulations**

Computational approaches, in particular molecular dynamics (MD) simulations, have been increasingly used to evaluate the interaction of drugs with the cell membrane.<sup>[75–77]</sup> The interaction of lead complexes **1** and **4** with a membrane model was studied using MD simulations, to evaluate the impact of specific chemical groups, introduced in the Cp ring (hydrazide or acetyl groups, respectively), of the reference complex **TM34**, in its mode of interaction with the cell membrane. In particular, their effects on the membrane insertion depth, preferred orientation, and membrane permeation, and consequently relate them to the cytotoxic activities. We applied the same protocols to all compounds so that a direct comparison between **TM34** and its derivatives leads to a significant error cancellation, hence providing a reliable quantification of the studied effects. These two complexes are representative of the two groups used to functionalize **TM34** (hydrazide and ketone). To study the preferred partitioning region and orientation of complexes **1** and **4**, we performed unrestrained MD simulations of each compound in the presence of a POPC bilayer membrane. In general, all complexes showed a clear preference towards the membrane phase, similar to **TM34**. They reached a stable insertion position just below the average position of phosphorous atoms, within the initial 200–350 ns of simulation (Figure 6A and S10). Most structural properties were equilibrated after these initial time segments (Figures S11–S13). None of the compounds showed membrane crossing or exiting events in our MD simulations, suggesting that these average insertion values correspond to energy minima. It should be noted that the polarity and/or the hydrogen-donor ability of the substituent group influences the insertion depth, which decreases as the polarity (and hydrogen-bonding with the lipid phosphate groups) increases, following the order: **TM34** (7 Å) > complex **4** (6 Å) > complex **1** (4 Å). (Figure 6B). Although these are small membrane-insertion differences, given the size of the phospholipid bilayer thickness, they are most likely related to different membrane partition profiles, which may help interpret the compounds' distinct cytotoxicity values. We implemented an Umbrella Sampling scheme coupled to MD simulations to study the complete membrane-crossing process of **TM34** and complexes **1** and **4**. This approach provided detailed structural information on the compounds and the POPC membrane at all steps of the insertion pathway (Figure S14). The sampling obtained for the compound positions in each

umbrella is very good with significant histogram overlap observed between them (Figure S15). The membrane deformations, observed in the US protocol, especially at more inserted umbrellas, are larger but can be easily correlated with the needed water desolvation process (Figures S16 and S17). The complexes' angle profiles and rotational tumbling also seem to be stable throughout the simulations (Figures S18 – S20). This stability is particularly important when calculating the energetics associated with the membrane-crossing process. We calculated the potential of mean force (PMF) energy profiles of all compounds (Figure 6C) which confirmed their strong preference towards the membrane phase, with a clear energy minimum located deep below the average phosphorous region (umbrellas 1.3–1.4). The energy barrier for membrane crossing (the difference between the profile minimum and the maximum at the membrane center) is significant, which is in agreement with the fact that we did not observe membrane-crossing events in the unrestrained MD simulations of these compounds. Despite having very similar PMF profiles, we still observed that complex **1** has a slightly higher energy barrier, its hydrazide substitution can establish more stabilizing interactions with the lipid headgroups. This is also in line with its smaller average insertion value, obtained from unrestrained MD. The membrane permeability coefficients (Pm) were calculated using the ISDM formalism (Figure 6D) where the POPC bilayer is considered symmetrical so that the resulting PMF energy profiles can be duplicated. Although the absolute values of Pm cannot be directly compared with those observed in cells,<sup>[78]</sup> their relative differences should provide strong hints on the membrane crossing abilities of each compound. We observed that complex **1** has a smaller Pm than **TM34**, which is in agreement with its structural properties and PMF energy profile. Finally, it should be noted that these complexes are cations and their calculated Pm values are still remarkably high and comparable with most hydrophobic drugs.<sup>[79–81]</sup>

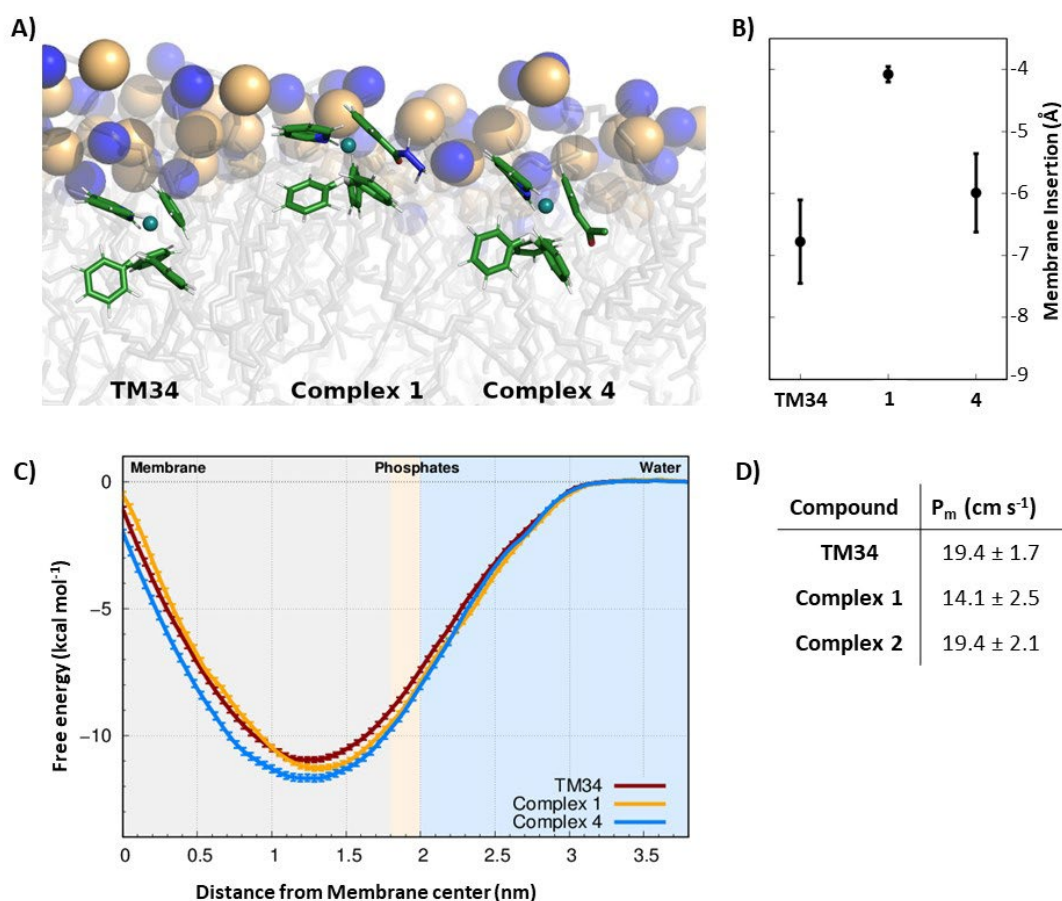


**Figure 5.** (A) Representation of the complexes at their preferred insertion depths. The structures correspond to conformations presenting each compound's preferred orientation. The POPC lipid tails are shown with transparent gray sticks with the phosphorus and nitrogen atoms represented as spheres (yellow and blue, respectively). (B) Average membrane insertion values for each compound. Insertion was calculated along the membrane normal vector, using the average position of the phosphorus atoms of the interacting monolayer as reference. Negative values correspond to the membrane-inserted positions, below the average phosphate region. The error bars show the standard deviation of the insertion. (C) Potential of mean force energy profile for the three compounds studied and using the water phase as the zero-energy reference. The light blue and light gray regions of the plot correspond to the water and membrane interior phases, respectively. The lipid phosphate group region (light pink) separates these two phases and is located at ~1.9 nm from the membrane center. The PMF error values were calculated from the standard error of the mean between the three replicates. (D) Permeability coefficients ( $P_m$ ) of the three compounds studied, calculated using the ISDM method. The error values were calculated from a jackknife leave-one-out strategy using the information from the three replicates.

## Conclusion

In summary, four novel ruthenium-peptide conjugates **RuPC1** – **RuPC4** were synthesized by incorporating an FGFR-targeting peptide, a cytotoxic Ru-cyclopentadienyl complex, and a pH-sensitive linker. These bi-functional RuPCs were rationally designed to selectively target FGFR-positive breast cancer cells and release *in situ* the cytotoxic Ru complex in a controlled way, allowing inhibition of cancer cells proliferation with reduced side cytotoxicity to normal cells. For all RuPCs, the cytotoxicity is correlated with the level of FGFR expression and presented selectivity for FGFR(+) breast cancer lines compared to normal fibroblasts. Importantly, the

cytotoxicity and drug release profiles of RuPCs were shown to be strongly dependent on the peptide conjugation position in the Ru complex and on the chemical environment around the hydrazone bond. It was possible to identify a lead bi-functional RuPC that holds the potential as an FGFR-targeted chemotherapeutic agent. This RuPC is sufficiently stable at neutral pH with a small percentage of drug release, and it achieves fast and almost complete drug release under mildly acidic conditions, such as the pH found in the tumor microenvironment. Overall, these promising results encourage us to further investigate the use of these bi-functional RuPCs as a novel platform for targeted chemotherapy of FGFR-positive breast cancers.

### Conflicts of interest

The authors declare no competing financial interests.

### Acknowledgments

We thank the Fundação para a Ciência e Tecnologia (FCT), I.P./MCTES for the financial support through the projects PTDC/QUI-QIN/0146/2020, UIDB/00100/2020 (CQE), LA/P/0056/2020 IMS), UIDB/04046/2020, UIDP/04046/2020 (BioISI), and for doctoral grant SFRH/BD/135915/2018 (J.F.M.) and 2023.01155.BD (I.P.). FCT, POPH and FSE- European Social Funds are acknowledged for the Individual Call to Scientific Employment Stimulus projects 2022/00028/CEECIND (T.S.M.), 2020/02383/CEECIND (J.A.S.C) and CEECIND/02300/2017 (M.M.) Work at IQF-CSIC supported by grant PID2020-112821GB-I00 from MCINN/AEI/10.13039/501100011033 to M.A.J. NMR experiments were performed at the Manuel Rico NMR laboratory (LMR) of the Spanish National Research Council (CSIC), a node of the Spanish Large-Scale National Facility (ICTS R-LRB).

### References

- [1] B. S. Chhikara, K. Parang, *Chemical Biology Letters* **2023**, *10*, 451–451.
- [2] H. Sung, J. Ferlay, R. L. Siegel, M. Laversanne, I. Soerjomataram, A. Jemal, F. Bray, *CA Cancer J Clin* **2021**, *71*, 209–249.
- [3] R. L. Siegel, K. D. Miller, H. E. Fuchs, A. Jemal, *CA Cancer J Clin* **2022**, *72*, 7–33.
- [4] S. Sauer, D. R. Reed, M. Ihnat, R. E. Hurst, D. Warshawsky, D. Barkan, *Front Oncol* **2021**, *11*, 659963.
- [5] B. Weigelt, J. L. Peterse, L. J. Van't Veer, *Nature Reviews Cancer* **2005**, *5*, 591–602.
- [6] J. Lu, P. S. Steeg, J. E. Price, S. Krishnamurthy, S. A. Mani, J. Reuben, M. Cristofanilli, G. Dontu, L. Bidaut, V. Valero, G. N. Hortobagyi, D. Yu, *Cancer Res* **2009**, *69*, 4951–4953.
- [7] X. Jiang, G. Chen, L. Sun, C. Liu, Y. Zhang, M. Liu, C. Liu, *Front Oncol* **2022**, *12*, 977226.
- [8] S. Navid, C. Fan, P. O. Flores-Villanueva, D. Generali, Y. Li, *Int J Mol Sci* **2020**, *21*, DOI 10.3390/IJMS21062011.
- [9] M. A. Krook, J. W. Reeser, G. Ernst, H. Barker, M. Wilberding, G. Li, H. Z. Chen, S. Roychowdhury, *British Journal of Cancer* **2020**, *124*, 880–892.

- [10] I. S. Babina, N. C. Turner, *Nature Reviews Cancer* **2017** *17*:5 **2017**, *17*, 318–332.
- [11] E. Witsch, M. Sela, Y. Yarden, *Physiology (Bethesda)* **2010**, *25*, 85–101.
- [12] R. Porta, R. Borea, A. Coelho, S. Khan, A. Araújo, P. Reclusa, T. Franchina, N. Van Der Steen, P. Van Dam, J. Ferri, R. Sirera, A. Naing, D. Hong, C. Rolfo, *Crit Rev Oncol Hematol* **2017**, *113*, 256–267.
- [13] J. Perez-Garcia, E. Muñoz-Couselo, J. Soberino, F. Racca, J. Cortes, *Breast* **2018**, *37*, 126–133.
- [14] S. Wang, Z. Ding, *Tumour Biol* **2017**, *39*, DOI 10.1177/1010428317698370.
- [15] Y. K. Chae, K. Ranganath, P. S. Hammerman, C. Vaklavas, N. Mohindra, A. Kalyan, M. Matsangou, R. Costa, B. Carneiro, V. M. Villaflor, M. Cristofanilli, F. J. Giles, *Oncotarget* **2017**, *8*, 16052–16074.
- [16] C. Pottier, M. Fresnais, M. Gilon, G. Jérusalem, R. Longuespée, N. E. Sounni, *Cancers (Basel)* **2020**, *12*, DOI 10.3390/CANCERS12030731.
- [17] S. B. Kim, F. Meric-Bernstam, A. Kalyan, A. Babich, R. Liu, T. Tanigawa, A. Sommer, M. Osada, F. Reetz, D. Laurent, S. Wittemer-Rump, J. Berlin, *Target Oncol* **2019**, *14*, 591–601.
- [18] Z. Xie, T. Fan, J. An, W. Choi, Y. Duo, Y. Ge, B. Zhang, G. Nie, N. Xie, T. Zheng, Y. Chen, H. Zhang, J. S. Kim, *Chem Soc Rev* **2020**, *49*, 8065–8087.
- [19] J. F. Machado, J. D. G. Correia, T. S. Morais, *Molecules* **2021**, *26*, 3153.
- [20] D. Chen, V. Milacic, M. Frezza, Q. Dou, *Curr Pharm Des* **2009**, *15*, 777–791.
- [21] M. Mladenović, I. Morgan, N. Ilić, M. Saoud, M. V. Pergal, G. N. Kaluđerović, N. Knežević, *Pharmaceutics* **2021**, *13*, DOI 10.3390/PHARMACEUTICS13040460.
- [22] Z. Zhao, X. Tao, Y. Xie, Q. Lai, W. Lin, K. Lu, J. Wang, W. Xia, Z. W. Mao, *Angewandte Chemie International Edition* **2022**, *61*, e202202855.
- [23] Y. Zhang, W. Zheng, Q. Luo, Y. Zhao, E. Zhang, S. Liu, F. Wang, *Dalton Transactions* **2015**, *44*, 13100–13111.
- [24] J. Liu, X. Liao, K. Xiong, S. Kuang, C. Jin, L. Ji, H. Chao, *Chemical Communications* **2020**, *56*, 5839–5842.
- [25] G. Lv, L. Qiu, K. Li, Q. Liu, X. Li, Y. Peng, S. Wang, J. Lin, *New Journal of Chemistry* **2019**, *43*, 3419–3427.
- [26] B. Bertrand, M. A. O’Connell, Z. A. E. Waller, M. Bochmann, *Chemistry – A European Journal* **2018**, *24*, 3613–3622.
- [27] A. M. Vargason, A. C. Anselmo, S. Mitragotri, *Nature Biomedical Engineering* **2021** *5*:9 **2021**, *5*, 951–967.
- [28] O. M. Kutova, E. L. Guryev, E. A. Sokolova, R. Alzeibak, I. V. Balalaeva, *Cancers (Basel)* **2019**, *11*, DOI 10.3390/CANCERS11010068.

- [29] G. Liu, L. Yang, G. Chen, F. Xu, F. Yang, H. Yu, L. Li, X. Dong, J. Han, C. Cao, J. Qi, J. Su, X. Xu, X. Li, B. Li, *Front Pharmacol* **2021**, *12*, 735446.
- [30] I. Ojima, *Acc Chem Res* **2008**, *41*, 108–119.
- [31] J. Bhattacharyya, J. J. Bellucci, I. Weitzhandler, J. R. McDaniel, I. Spasojevic, X. Li, C. C. Lin, J. T. A. Chi, A. Chilkoti, *Nature Communications* **2015** *6:1* **2015**, *6*, 1–12.
- [32] S. F. A. Rizvi, N. Abbas, H. Zhang, Q. Fang, *J Med Chem* **2023**, *66*, 8324–8337.
- [33] Q. Song, X. Chuan, B. Chen, B. He, H. Zhang, W. Dai, X. Wang, Q. Zhang, *Drug Deliv* **2016**, *23*, 1734–1746.
- [34] L. Ayalew, J. Acuna, S. F. Urfano, C. Morfin, A. Sablan, M. Oh, A. Gamboa, K. Slowinska, *ACS Med Chem Lett* **2017**, *8*, 814–819.
- [35] L. Hou, T. Zhong, P. Cheng, B. Long, L. Shi, X. Meng, H. Yao, *Front Bioeng Biotechnol* **2022**, *10*, 938662.
- [36] C. Zhang, D. Pan, K. Luo, W. She, C. Guo, Y. Yang, Z. Gu, *Adv Healthc Mater* **2014**, *3*, 1299–1308.
- [37] L. Gong, H. Zhao, Y. Liu, H. Wu, C. Liu, S. Chang, L. Chen, M. Jin, Q. Wang, Z. Gao, W. Huang, *Acta Pharm Sin B* **2023**, DOI 10.1016/J.APSB.2023.02.013.
- [38] M. Mazel, P. Clair, C. Rousselle, P. Vidal, J. M. Scherrmann, D. Mathieu, J. Tamsamani, *Anticancer Drugs* **2001**, *12*, 107–116.
- [39] R. Li, / Dalton, J. F. Machado, T. S. Morais, D. Transactions, *Dalton Transactions* **2022**, *51*, 2593–2609.
- [40] V. P. Chavda, H. K. Solanki, M. Davidson, V. Apostolopoulos, J. Bojarska, *Molecules* **2022**, *27*, DOI 10.3390/MOLECULES27217232.
- [41] P. Hoppenz, S. Els-Heindl, A. G. Beck-Sickinger, *Front Chem* **2020**, *8*, 545283.
- [42] K. S. Gkika, D. Cullinane, T. E. Keyes, *Topics in Current Chemistry* **2022** *380:5* **2022**, *380*, 1–48.
- [43] L. C. C. Lee, L. Huang, P. K. K. Leung, K. K. W. Lo, *Eur J Inorg Chem* **2022**, *2022*, e202200455.
- [44] M. Soler, L. Feliu, M. Planas, X. Ribas, M. Costas, *Dalton Transactions* **2016**, *45*, 12970–12982.
- [45] V. Moreno, M. Font-Bardia, T. Calvet, J. Lorenzo, F. X. Avilés, M. H. Garcia, T. S. Morais, A. Valente, M. P. Robalo, *J Inorg Biochem* **2011**, *105*, 241–249.
- [46] A. I. Tomaz, T. Jakusch, T. S. Morais, F. Marques, R. F. M. De Almeida, F. Mendes, É. A. Enyedy, I. Santos, J. C. Pessoa, T. Kiss, M. H. Garcia, *J Inorg Biochem* **2012**, *117*, 261–269.
- [47] L. Côte-Real, A. P. Matos, I. Alho, T. S. Morais, A. I. Tomaz, M. H. Garcia, I. Santos, M. P. Bicho, F. Marques, *Microscopy and Microanalysis* **2013**, *19*, 1122–1130.



- [48] L. Côrte-Real, F. Mendes, J. Coimbra, T. S. Morais, A. I. Tomaz, A. Valente, M. H. Garcia, I. Santos, M. Bicho, F. Marques, *Journal of Biological Inorganic Chemistry* **2014**, *19*, 853–867.
- [49] J. Franco Machado, M. Machuqueiro, F. Marques, M. P. Robalo, M. F. M. Piedade, M. H. Garcia, J. D. G. Correia, T. S. Morais, *Dalton Transactions* **2020**, *49*, 5974–5987.
- [50] R. D. M. Silva, J. F. Machado, K. Gonçalves, F. M. Lucas, S. Batista, R. Melo, T. S. Morais, J. D. G. Correia, *Molecules* **2021**, *26*, 7349.
- [51] F. Hollósy, T. Lóránd, L. Örfi, D. Erös, G. Kéri, M. Idei, *Journal of Chromatography B* **2002**, *768*, 361–368.
- [52] A. Berthod, S. Carda-Broch, *J Chromatogr A* **2004**, *1037*, 3–14.
- [53] E. Villemin, Y. C. Ong, C. M. Thomas, G. Gasser, *Nat Rev Chem* **2019**, *3*, 261–282.
- [54] M. E. Davis, Z. Chen, D. M. Shin, *Nat Rev Drug Discov* **2008**, *7*, 771–782.
- [55] T. F. D. Silva, D. Vila-Viçosa, M. Machuqueiro, *J Chem Theory Comput* **2021**, *17*, 3830–3840.
- [56] M. Jin, Y. Yu, H. Qi, Y. Xie, N. Su, X. Wang, Q. Tan, F. Luo, Y. Zhu, Q. Wang, X. Du, C. J. Xian, P. Liu, H. Huang, Y. Shen, C. X. Deng, D. Chen, L. Chen, *Hum Mol Genet* **2012**, *21*, 5443–5455.
- [57] D. P. Perrault, G. K. Lee, S. Y. Park, S. Lee, D. Choi, E. Jung, Y. J. Seong, E. K. Park, C. Sung, R. Yu, A. Bouz, A. Pourmousa, S. J. Kim, Y. K. Hong, A. K. Wong, *Lymphat Res Biol* **2019**, *17*, 19–29.
- [58] B. Over, P. McCarren, P. Artursson, M. Foley, F. Giordanetto, G. Grönberg, C. Hilgendorf, M. D. Lee, P. Matsson, G. Muncipinto, M. Pellisson, M. W. D. Perry, R. Svensson, J. R. Duvall, J. Kihlberg, *J Med Chem* **2014**, *57*, 2746–2754.
- [59] L. Doedens, F. Opperer, M. Cai, J. G. Beck, M. Dedek, E. Palmer, V. J. Hruby, H. Kessler, *J Am Chem Soc* **2010**, *132*, 8115–8128.
- [60] O. Demmer, A. O. Frank, F. Hagn, M. Schottelius, L. Marinelli, S. Cosconati, R. Brack-Werner, S. Kremb, H. J. Wester, H. Kessler, *Angewandte Chemie International Edition* **2012**, *51*, 8110–8113.
- [61] Y. Shen, A. Bax, *J Biomol NMR* **2010**, *46*, 199–204.
- [62] M. Schubert, D. Labudde, H. Oschkinat, P. Schmieder, *J Biomol NMR* **2002**, *24*, 149–154.
- [63] D. S. Wishart, C. G. Bigam, A. Holm, R. S. Hodges, B. D. Sykes, *J Biomol NMR* **1995**, *5*, 67–81.
- [64] Q. He, J. Chen, J. Yan, S. Cai, H. Xiong, Y. Liu, D. Peng, M. Mo, Z. Liu, *Asian J Pharm Sci* **2020**, *15*, 416–448.
- [65] X. Dai, H. Cheng, Z. Bai, J. Li, *J Cancer* **2017**, *8*, 3131–3141.
- [66] S. E. Smith, P. Mellor, A. K. Ward, S. Kendall, M. McDonald, F. S. Vizeacoumar, F. J. Vizeacoumar, S. Napper, D. H. Anderson, *Breast Cancer Research* **2017**, *19*, 1–12.

- [67] D. L. Holliday, V. Speirs, *Breast Cancer Research* **2011**, *13*, 1–7.
- [68] R. N. Gomes, F. Manuel, D. S. Nascimento, *npj Regenerative Medicine* **2021**, *6*, 1–12.
- [69] A. Stunova, L. Vistejnova, *Cytokine Growth Factor Rev* **2018**, *39*, 137–150.
- [70] R. De Araújo, M. Lôbo, K. Trindade, D. F. Silva, N. Pereira, *Skin Pharmacol Physiol* **2019**, *32*, 275–282.
- [71] N. Abdian, P. Ghasemi-Dehkordi, M. Hashemzadeh-Chaleshtori, M. Ganji-Arjenaki, A. Doosti, B. Amiri, *Cell Tissue Bank* **2015**, *16*, 487–495.
- [72] A. V. Lee, S. Oesterreich, N. E. Davidson, *J Natl Cancer Inst* **2015**, *107*, DOI 10.1093/JNCI/DJV073.
- [73] K. Ji, C. Lee, B. G. Janesko, E. E. Simanek, *Mol Pharm* **2015**, *12*, 2924–2927.
- [74] I. Yildiz, *Journal of Physical Chemistry A* **2016**, *120*, 3683–3692.
- [75] A. I. Bunea, S. Harloff-Helleberg, R. Taboryski, H. M. Nielsen, *Adv Colloid Interface Sci* **2020**, *281*, 102177.
- [76] J. Guo, Y. Bao, M. Li, S. Li, L. Xi, P. Xin, L. Wu, H. Liu, Y. Mu, *Wiley Interdiscip Rev Comput Mol Sci* **2023**, e1679.
- [77] J. Sun, A. Kulandaisamy, J. Liu, K. Hu, M. M. Gromiha, Y. Zhang, *Comput Struct Biotechnol J* **2023**, *21*, 1205–1226.
- [78] A. M. M. Gomes, P. J. Costa, M. Machuqueiro, *BBA Advances* **2023**, *4*, 100099.
- [79] D. Vila-Viçosa, B. L. Victor, J. Ramos, D. Machado, M. Viveiros, J. Switala, P. C. Loewen, R. Leitao, F. Martins, M. Machuqueiro, *Mol Pharm* **2017**, *14*, 4597–4605.
- [80] J. B. Loureiro, R. Ribeiro, N. Nazareth, T. Ferreira, E. A. Lopes, A. Gama, M. Machuqueiro, M. G. Alves, L. Marabini, P. A. Oliveira, M. M. M. Santos, L. Saraiva, *Pharmacol Res* **2022**, *175*, 106026.
- [81] C. F. de Faria, T. Moreira, P. Lopes, H. Costa, J. R. Krewall, C. M. Barton, S. Santos, D. Goodwin, D. Machado, M. Viveiros, M. Machuqueiro, F. Martins, *Biomed Pharmacother* **2021**, *144*, DOI 10.1016/J.BIOPHA.2021.112362.